Ultrafast dynamics of bright and dark positive trions for valley polarization in monolayer WSe_{2}

Keisuke Shinokita, Xiaofan Wang, Yuhei Miyauchi, Kenji Watanabe, Takashi Taniguchi, Satoru Konabe, and Kazunari Matsuda

Phys. Rev. B **99**, 245307 — Published 25 June 2019

DOI: 10.1103/PhysRevB.99.245307

Ultrafast Dynamics of Bright and Dark Positive Trions for Valley Polarization in Monolayer WSe_2

Keisuke Shinokita[1,†], Xiaofan Wang[1], Yuhei Miyauchi[1], Kenji Watanabe[2], Takashi Taniguchi[2], Satoru Konabe[3], and Kazunari Matsuda[1,*]

[1]*Institute of Advanced Energy, Kyoto University, Uji, Kyoto 611-0011, Japan*

[2]*National Institute for Materials Science, 1-1 Namiki, Tsukuba, Ibaraki 305-0044, Japan*

[3]*Department of Chemical Science and Technology, Hosei University, Koganei, Tokyo 184-8584, Japan*

Abstract

Optical excited state dynamics of bright and dark positively charged excitons (positive trions) in 1-layer (1L-) WSe_2 were studied by a combination of time- and polarization-resolved photoluminescence and pump-probe spectroscopy. Bright positive trions showed ultrafast relaxation to dark positive trions (~1 ps) and to ground state (10±5 ps), while dark positive trions showed slow decay to the ground state (~300 ps) at 10 K. Under valley selective excitation with circularly polarized light, the valley relaxation time of the bright trions was 1.5±0.5 ns at 10 K, which is much longer than typical exciton valley relaxation times of 10 ps. This insight into the slower valley relaxation dynamics of positive trions suggests that the electron-hole exchange interactions that is dominant in neutral exciton valley relaxation, are suppressed by the presence of additional holes.

†shinokita.keisuke.4r@kyoto-u.ac.jp

*matsuda@iae.kyoto-u.ac.jp

Keywords: Valley polarization, transition metal dichalcogenides, charged exciton

Atomically thin transition metal dichalcogenides (TMDs) possess novel properties originating from their extremely low dimensionality, making monolayer TMDs an ideal platform for investigating fundamental physics in two-dimensional systems[1,2]. The two-dimensional character of monolayer TMD strongly enhances Coulomb interactions, which imparts extraordinarily large binding energies to bound electrons and holes (e–h) as neutral excitons, two-electrons and a hole ($2e$–h) as negatively charged excitons (negative trions), and an electron and two-holes (e–$2h$) as positively charged excitons (positive trions)[3–12]. These features result in novel optical and electrical properties dominated by the many-body excitonic effects in monolayer TMD. These highly stable neutral excitons and trions have valley degrees of freedom, because TMDs have a direct bandgap with a band-edge located at energy degenerate valleys (K, −K) at the corners of the hexagonal Brillouin zone[2,13–20]. The valley degrees of freedom coupled with the spin degrees of freedom originating from strong spin-orbit interactions and breaking of inversion symmetry enable selective photoexcitation of excitons and trions to the K or −K valleys with the use of circularly polarized light. These effects give rise to valley polarized excitons and trions (valley polarization).

Three-body trions are fascinating quasiparticles among valley excitonic phenomena because their net charge enables detection and manipulation by an electric field through the valley Hall effect[19]. In TMDs, positive trions have two states, denoted as optically bright and dark states, for which electron and hole spins in the same valley are oriented anti-parallel and parallel to each other, respectively. In tungsten-based TMDs (WS_2 and WSe_2), the dark state at the lower energy sides markedly influences the optical properties[21–23]. However, the role of the optically-forbidden dark state in optically

excited state dynamics and valley polarization has yet to be fully clarified. Recent research has examined dark trions in monolayer WSe_2 through the use of strong in-plane magnetic fields[24,25] and plasmonic effects[26,27]. However, because these techniques affect trion properties, direct probing of the intrinsic properties of dark trions is required. To the best of our knowledge, comprehensive studies of positive trion dynamics including bright and dark state and their role in the valley depolarization process have yet to be demonstrated.

In this paper, we studied the relaxation dynamics of bright and dark positive trions for valley polarization in 1-layer (1L-) WSe_2 with the use of combined time- and polarization-resolved photoluminescence (PL) and pump-probe spectroscopy. We reveal ultrafast relaxation from bright to dark trions (~1 ps) and slow decay of dark trions to the ground state (~300 ps) at 10 K. Notably, the valley relaxation time of the bright trions (>70 ps) is much longer than the typical exciton valley relaxation time (10 ps) at 10 K. Conversely, dark trions are equally distributed in the K and −K valley after the efficient population transfer from the bright trions with a large momentum.

We studied a mechanically exfoliated 1L-WSe_2. The number of WSe_2 layers was determined from the optical contrast and peak positions in the Raman and PL spectra[28–30]. To focus on positive trions, a field-effect transistor (FET) was fabricated from a 1L-WSe_2 layer by a dry-transfer method onto Pt electrodes on a SiO_2/Si substrate with an SiO_2 layer thickness of 270 nm. The device was covered by hexagonal boron nitride (*h*-BN). A

back-gate voltage V_{Gate} was applied to inject holes into the 1L-WSe_2. The doped carrier density n under a gate voltage V_{Gate} was estimated from the relationship of the geometric capacitance and the back-gate voltage using $n \approx |V_{\mathrm{Gate}}|\varepsilon\varepsilon_0/t_{\mathrm{SiO_2}}$, where ε=3.9 is the dielectric constant of silicon dioxide, ε_0 is the dielectric constant of vacuum, and $t_{\mathrm{SiO_2}}$ is the thickness of SiO_2[31]. Through the use of the above relationship, the doped hole density at gate voltages of −40 V was estimated to be 2×10^{12} cm^{-2}.

In the polarization-resolved pump-probe experiments, a σ_+ circularly polarized pump pulse excites the 1L-WSe_2, then a delayed σ_+ and σ_- circularly polarized probe pulse measures the change of reflectivity as a function of pump-probe delay times. A ~200-fs pump pulse having a center photon energy of 1.824 eV was generated by an optical parametric amplifier from the output of a femtosecond laser with a repetition rate of 1 MHz. A probe pulse of ~350 fs having photon energies between 1.6 and 2.3 eV duration was generated by a nonlinear process in YAG crystals. The average pump power of 1 μW was focused to a spot diameter of 2 μm with the use of a 100× objective lens (NA = 0.55). The excitation density of $N \approx 10^{12}$ /cm^2 electron-hole pairs in 1L-WSe_2 is in the linear regime[32]. The reflected probe light was detected with a photodiode after passing through a monochromator. The electrical signal from the reflectance change induced by the pump-pulse was fed into a lock-in amplifier at a chopping frequency of ~800 Hz.

Polarization-resolved PL was measured with a continuous wave He–Ne laser (photon energy of 1.959 eV, power of 10 μW). Time-resolved PL spectroscopy was conducted by

time-correlated single-photon counting (TCSPC), where the 1L-WSe_2 was excited by a pulsed supercontinuum light source (photon energy of 1.922 eV, power of 45 μW, pulse duration of ~20 ps, and repetition rate of 40 MHz). The temperature of 1L-WSe_2 was controlled by a cryogen-free cryostat.

Figure 1(a) shows a schematic diagram of the band structure of 1L-WSe_2 with an out-of-plane valley-contrasting spin splitting in valence and conduction bands owing to the strong spin-orbit interaction. The valence-band splitting of 450 meV is much larger than the conduction-band splitting of 40 meV[33]. Because the bottom of the conduction band and the top of the valence band have opposite spin configuration in 1L-WSe_2, the interband transition from the first-valence band (VB1) to the first-conduction band (CB1) is optically forbidden but allowed to the second-conduction band (CB2), as shown in Fig. 1(a). The two transitions from VB1 to CB2 (red arrow) and from second-valence band (VB2) to CB1 (green allow) are denoted A and B transitions, respectively[1,14]. In addition, the opposite spin configurations for the K and −K valleys enable the optical selection rules for interband transitions with valley-selective excitation of electron-hole pairs via circularly polarized light, and the optically oriented valley polarization can be detected by circular polarization of the PL signals.

Under hole-doped conditions two valley configurations of positively charged excitons (positive trions) including spin-allowed bright and -forbidden dark states are possible as illustrated in Fig. 1(b). The spin-allowed bright trions efficiently couple to light,

whereas spin-forbidden dark trions do not couple to light, and usually have much longer recombination lifetime than those of the bright trions. The two trion states can be probed with the use of combined PL and pump-probe signals of A and B transitions: The PL measurements probe the recombination process of the bright state, whereas the B transitions probe the dark state population because the final state of the B transition (CB1 band) is occupied by electrons forming the dark trions and the formation and change of the wavefunction of the dark trions affect the transition. The A transitions monitor the hole population in the VB1 band, which reflects both bright and dark trion populations because the initial state of the transition (VB1) band is occupied by holes that form bright and dark trions. The population decay of the bright and dark trions reduces the VB1 hole population. To date, the A and B transition features have been used to investigate the optically allowed and forbidden state of neutral excitons[34] and negative trions[35].

Figure 1(c) shows differential reflectance spectra $\delta R/R = (R_{\mathrm{Sample}} - R_{\mathrm{Silicon}})/R_{\mathrm{Silicon}}$ of 1L-WSe_2 on a SiO_2/Si substrate at 10 K with a gate voltage of −40 V based on the reflectance of 1L-WSe_2 (R_{Sample}) and the silicon substrate (R_{Silicon}). Optically excited electron-holes capture excess holes electrostatically-injected into the 1L-WSe_2, forming positively charged excitons (positive trions). We observed a dispersive feature near 1.72 eV from positive trions (T^+) owing to the A transition from VB1 to CB2[36]. Another peak was observed near 2.14 eV. We assigned this peak to the B transition from VB2 to CB1. The energy difference between the A and B transitions of ~420 meV is mainly determined by the energy splitting of the valence-band of 450 meV.

Figure 1(d) shows the polarization-resolved PL spectra with gate voltages of −40 V at 10 K under σ_+ excitation corresponding to K valley excitation. A prominent emission appeared near 1.72 eV, which originated from recombination of the bright positive trions (T^+)[36]. The emission peak at 1.67 eV appears to originate from localized excitons at defect states[15,36,37]. The σ_+ component of the PL spectra of the trion (red curve) has a higher intensity than the σ_- component of the PL spectra (black curve). The optically generated trions at the K valley are more populated in the pumped K valley, which corresponds to the valley polarized bright trion state in 1L-WSe_2 (valley polarization). The valley polarization ρ can be estimated as $\rho = (I_{\sigma_+} - I_{\sigma_-})/(I_{\sigma_+} + I_{\sigma_-})$, where $I_{\sigma+}$ and $I_{\sigma-}$ are the trion PL intensities of the σ_+ and σ_- components, respectively. The valley polarization ρ of positive trions was estimated to be approximately 0.3 at 10 K.

Figure 1(e) shows the time-resolved PL decays of the positive trions under −40 V at 10 K (red circles), as well as the instrumental response function (IRF) of the setup (black curve). The PL transients are fitted with a single-exponential decay function as $I = A\exp(-t/\tau)$ convoluted with the IRF, as shown by the green curve, which gives a bright trion lifetime of 10±5 ps. Similar decay times of trion PL emission have been reported[15,38,39].

Ultrafast dynamics of the bright and dark trions in 1L-WSe_2 were studied further by two-color helicity-resolved pump-probe spectroscopy at 10 K. Figure 2(a) shows the

time development of polarization-resolved transient differential reflectance spectra probed around the B transition with σ_+ polarization by pump pulse with σ_+ polarization. The pump energy of 1.824 eV was tuned to be above the A transition and below the B transitions so that electrons and holes were excited to CB2 and VB1 in the K valley, respectively. The transient reflectance signals of the B transition were observed even for the lower optical excitation around the A transition. Figure 2(c) shows the transient spectra at different delay times. The observed reflectance changes are simply attributed to the decrease of absorption caused by the Pauli-exclusion principle (state-filling effect) originating from photoexcited electrons in the CB1 band, and there were no peak shifts in the transient reflectance over time. Figure 2(e) shows the decay profiles of the transient differential reflectance at 2.12 eV. As shown in the inset of the Fig. 2(e), the reflectance changes rise within a finite time of approximately 1 ps, suggesting ultrafast electron relaxation from the excited CB2 to CB1 state and transformation from bright to dark trions. After reaching the maximum, the reflectivity change showed a slower decay on the order of several hundred ps. The decay constant of 300 ps determined by fitting the decay profiles with a single exponential decay function corresponds to dark trion relaxation time.

Figure 3(a) shows the time development of polarization-resolved transient differential reflectance spectra of σ_+ component probed around the A transition after the arrival of the pump pulse with σ_+ polarization. Figure 3(c) shows the transient spectra at various delay times. The σ_+ component shows the asymmetric spectral change. The differential reflectance spectra were analyzed considering the decrease of absorption

(bleaching) and the shift of the peak energy[40]. The analyzed differential reflectance spectra indicated by the shaded areas in Fig. 3(c) almost reproduced the experimentally obtained results. The differential reflectance spectra of the σ_+ component derived from both the absorption bleaching and the shift of the peak energy. Figure 3(e) shows the time-development of the extracted bleaching contribution for the σ_+ component after fitting (red circles). The time-development of the bleaching of the σ_+ component showed bi-exponential decay with fast and slow components. The fitting of the transient with a bi-exponential decay results in a fast decay component of ~10 ps and a slow decay component of ~300 ps, which is consistent with the bright trion decay of 10±5 ps in the PL measurements and the dark trion decay of ~300 ps in the B transition, respectively. This is because the pump-probe signals of the A transition reflect the bright and dark trion populations, as stated above.

Figure 4 summarizes the intravalley bright and dark trion dynamics suggested by the transient differential reflectivity and time-resolved PL measurements. The schematics of trion dynamics in the many-body (trion) and one-electron picture are shown in Fig. 4(a) and 4(b), respectively. The optically excited electron-hole pairs capture electrostatically-injected holes to form bright trions. The fomration of bright trions is expected to be occurring within the time resolution of ~350 fs because of strong Coulomb interaction[41]. The bright trions suffers radiative decay to the ground state on the time scale of 10±5 ps, while the population transfer from bright trions to dark trions also happens on the order of 1 ps. Finally, the dark trions decay nonradiatively to the ground state on the time scale of ~300 ps.

The two relaxation pathways of the bright trions, including the transformation to dark trions (~1 ps) and radiative recombination (10±5 ps) suggest a momentum dependent scattering process of the bright trions. The dark trion formation requires a spin-flip process, and is thus expected to be slower than radiative recombination, although this is the case only at the minimum of K valley ($k \approx 0$). The optically generated bright trions in nonequilibrium conditions immediately after the photoexcitation because of the finite laser energy bandwidth, are thermalized to be continuously distributed both around and away from the minimum of the K valley ($k \approx 0$ and $k > 0$, respectively) within ~100 fs due to carrier-carrier scattering[42]. The observed fast transformation to dark (~1 ps) trions on the similar timescale of carrier-phonon scattering process[42] indicates that the phonon scattering process causes not only intravalley-cooling of the carriers to Fermi-Dirac distribution around the minimum of the CB2 ($k \approx 0$) determined by the lattice temperature, but also spin-flip intervalley-scattering to the CB1 band. The cooled carriers around the minimum of the CB2 are stable against the spin-flip scattering, resulting in the radiative decay to ground state on the timescale of 10±5 ps. Such momentum dependent scattering processes are consistent with the reported ultrafast spin-flip process for neutral excitons in monolayer WS_2[34].

The helicity-resolved PL and pump-probe signals give additional information on the valley dynamics. Phenomenologically, the valley polarization ρ in the time-integrated PL measurement is expressed as[14,36,43–46]

$$\rho = \frac{\rho_0}{1 + \frac{\langle \tau_T \rangle}{\tau_v}}, \#(1)$$

where ρ_0 is the initial valley polarization created by the circularly polarized light, $\langle \tau_T \rangle$ is the mean trion lifetime, and τ_v is the valley relaxation time between K and −K valleys. Here, we calculated the value of ρ_0 to be ~0.35 from polarization-resolved PL decay measurements[47]. From the time-resolved PL decay measurements, as shown in Fig. 1(e), the trion lifetime $\langle \tau_T \rangle$ is given as 10±5 ps. Through the use of Eq. (1) and the experimentally obtained parameters, the nearly same value of ρ_0 and ρ suggests the much longer valley relaxation time of 1.5±0.5 ns than the trion lifetime of 10±5 ps. The valley relaxation time of bright trions at 10 K is at least longer than the relaxation time at 50 K of 70 ps[48], which is longer than the valley relaxation time of excitons of approximately 10 ps at 10 K[46].

Figure 2(b) and (d) show the transient reflectance signals probed around the B transition for the σ_+ and σ_- components, respectively. The transient reflectivity of the σ_+ and σ_- components showed almost identical changes, reflecting the same population of electrons of CB1 at the K and −K valleys. The time-development of the transient reflectance for σ_- components, as shown in the Fig. 2(c) (black diamonds), also indicated identical time-development to that of the σ_+ component (red circles). Figure 3(b) and (d) show the transient reflectance signals probed around the A transition for the σ_+ and σ_- components, respectively. In contrast to the differential reflectance change of the B transition, the differential reflectance spectra of the A transition showed notable differences between the σ_+ and σ_- components. The fitting procedure revealed that the σ_- component derived mainly from the absorption bleaching [filled lines in Fig. 3(d)].

Figure 3(e) shows the time-development of the bleaching signal for the σ_- component after fitting (black diamonds). This was a common bi-exponential decay as the σ_+ component, although the intensity of bleaching was different. The inset shows the difference between the σ_+ and σ_- components, indicating a long-lasting difference on a time scale longer than that measured by our setup (>800 ps).

In the B transition pump-probe measurement, the σ_+ (σ_-) probe pulse monitors the unpumped −K (pumped K) valley because the CB1 and VB2 has the opposite spin configuration to that of CB2 and VB1, respectively. As shown in Fig. 2(e), the σ_+ and σ_- components show identical signals, meaning that the photoexcited electrons relax to CB1 in the K and −K valleys equally and the dark trions are not valley polarized. Conversely, in the A transition pump-probe measurement, the σ_+ components show larger bleaching signals [Fig. 3(e)] with an additional peak shift compared with the σ_- components, where the σ_+ (σ_-) probe reflects the pumped K (unpumped −K) valley information. The transient peak shift in the pumped K valley is thought to be caused by bandgap renomarlization[49,50] and an increase of the Fermi level by optically excited electrons and holes[51] after ~1 ps. The existence of the energy shift only in the pumped K valley suggests that holes are not intervalley-scattered to the unpumped –K valley. The population unbalance of long-lived spin-polarized holes at the K and –K valleys induces long-lasting differences of the bleaching signals of the σ_+ and σ_- components with lifetimes of >800 ps[52], which is consistent with previous Kerr rotation measurements[38,53–55].

Figure 4 also summarizes the intervalley bright and dark trion dynamics. The optical excitation of electron-hole pairs in the K valley under hole doping causes initial ultrafast decay into bright trions in the K and −K valleys, which determines the initial valley polarization ρ_0. The optically generated bright trions with large momentum ($k>>0$) undergo fast trion relaxation from bright to dark states with $\gamma_{k\neq 0}$ of (~1 ps)$^{-1}$, which results in efficient population transfer to dark states through phonon-assisted processes[34]. The other bright trions at the center of the K valley ($k\approx 0$) decay radiatively with Γ_b of (~10±5 ps)$^{-1}$. The bright trions also undergo intervalley scattering between the pumped K and unpumped −K valley on a time scale longer than 70 ps. Conversely, dark trions are equally distributed in the K and −K valley, and only decay nonradiatively to the ground state with a Γ_d of (~300 ps)$^{-1}$. Finally, the valley polarized holes suffer intervalley scattering to reach an initial condition with valley-nonpolarized holes on a time scale longer than 800 ps. The timescales of bright and dark positive trions are summarized in Table S1[56].

Having comprehensively clarified the valley dynamics, we next comment shortly on the valley relaxation process of positive bright trions. The valley relaxation time of trions (>70 ps) is longer than the valley relaxation time of excitons (~10 ps)[46]. In the case of neutral excitons, momentum-dependent long-range electron-hole exchange interactions have been shown to be dominant in valley relaxation[14,45,57–61]. As a first step, the exchange interaction in the valley relaxation process of the positive trions is discussed by considering the effects of excess holes. The hole doping would reduce the trion oscillator strength because of the Pauli blocking effect[62]. Because the strength of

the exchange interaction is proportional to the oscillator strength[63], the off-diagonal coupling between different valley configurations in exchange interactions are suppressed for positive trions[23]. Furthermore, the screening effect originating from doped carriers might also reduce the exchange interaction[46]. The suppressed exchange interaction under hole doping would slow down valley relaxation, which qualitatively explains the observed long valley relaxation of positive trions.

In summary, we studied the relaxation dynamics of bright and dark positive trions for valley polarization in 1L-WSe_2. We reveal ultrafast relaxation from bright to dark trions (~1 ps) and slow decay of dark trions to the ground state (~300 ps) at 10 K. We also found that the valley relaxation time of the bright trions (> 70 ps) was much longer than the typical exciton valley relaxation time (10±5 ps). These insights into the valley dynamics of positive trions indicate that electron-hole exchange interactions are suppressed by additional holes in three-body trion systems. The valley dynamics of the positive trion systems reported here provide further motivation for microscopic theoretical studies on many body effects and valley dependent exchange interactions, which are pronounced in emergent monolayer semiconductors.

This work was supported by JSPS KAKENHI (Grant Numbers JP24681031, JP16H00911, JP15K13337, JP15H05408, JP15K13500, JP16H00910, JP16H06331, and JP17H06786), by the Keihanshin Consortium for Fostering the Next Generation of Global Leaders in Research (K-CONNEX) established by the Human Resource Development Program for Science and Technology, MEXT, ATI Research Grants 2017,

and by the Asahi Glass Foundation.

Figure captions

Figure 1. (a) Schematic illustration for the A (B) transition in WSe_2 corresponding to a transition from the spin-orbit-split VB1 (VB2) valence band to CB2 (CB1) conduction band. (b) Valley configurations of positively charged exciton (positive trion) including bright and dark states in K valley in monolayer WSe_2. Red (green) line denotes spin-up (spin-down) conduction and valence bands. The remaining configurations are the time reversal of those shown in the figure (−K bright and dark trions). (c) Differential reflectance spectrum measured at 10 K at gate voltage of −40 V. Dispersive features around 1.7 and 2.1 eV correspond to the A and B transitions, respectively, as shown in Fig. 1(b). (d) Polarization-resolved PL spectra under σ_+ excitation at 10 K at a gate voltage of −40 V. The red and black curves show the σ_+ and σ_- PL intensities, respectively. (e) Time-resolved PL decay profiles of positive trions measured at 10 K under the gate voltage of −40 V (open circles), and fitting results with convolution of exponential decay with the instrumental response function (IRF) (green curve). Black curve shows the IRF. Inset illustrates the configuration of the bright trion recombination process, which dominates the PL signal.

Figure 2. (a, b) Time- and probe-energy resolved transient differential reflectance around the B transition at the gate voltage of −40 V with different delay times at 10 K. The pump pulse is σ_+ circularly polarized and the probe pulses are σ_+ and σ_- circularly polarized for (a) and (b), respectively. (c, d) Transient differential reflectance spectra probed at the B transition at the gate voltage of −40 V with different delay times at 10 K. (e) Decay profiles of the transient differential reflectance at 2.12 eV. Solid curve shows

fitting results. Inset shows a close up of the early decay time. Inset illustrates the transition from bright to dark states at early delay times and the dark trion recombination process at later times, which determine the pump-probe signal at the B transition.

Figure 3. (a, b) Time- and probe-energy resolved transient differential reflectance around the A transition at the gate voltage of −40 V with different delay times at 10 K. The pump pulse is σ_+ circularly polarized and the probe pulses are σ_+ and σ_- circularly polarized for (a) and (b), respectively. (c, d) Transient differential reflectance spectra probed at the A transition at the gate voltage of −40 V with different delay times at 10 K (open circles). Solid lines are fitting results assuming bleaching and shift. (e) Decay profiles of the bleaching signal (red circles for σ_+ and black diamonds for σ_- probe). Solid curves are fitted by bi-exponential functions. Inset shows differences between the σ_+ and σ_- polarized probe signal (circles) and a guide to eye (line). Inset illustrates the configurations of the bright (dark) trion recombination process at early (later) delay times, which dominate the pump-probe signal at the A transition.

Figure 4. (a) Schematic of the intra- and intervalley relaxation processes of positive trions in the K valley excitation by circularly polarized light. (b) Schematic of the same valley relaxation process of electrons and holes in a one-electron band picture, and the respective time scales as measured in the experiment.

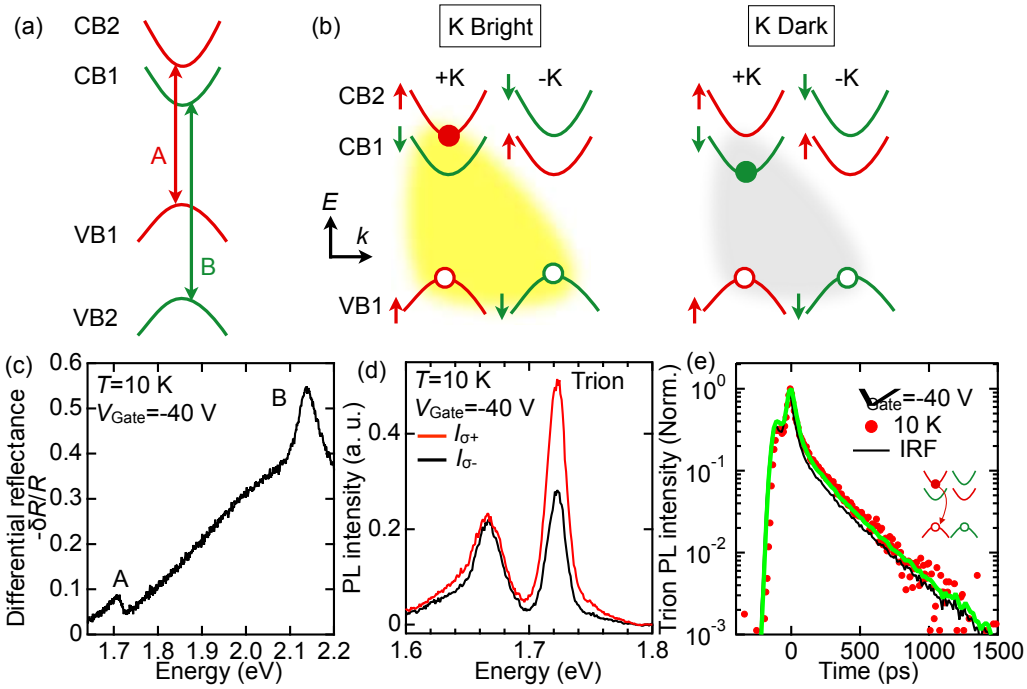

Figure 1 K. Shinokita *et al.*

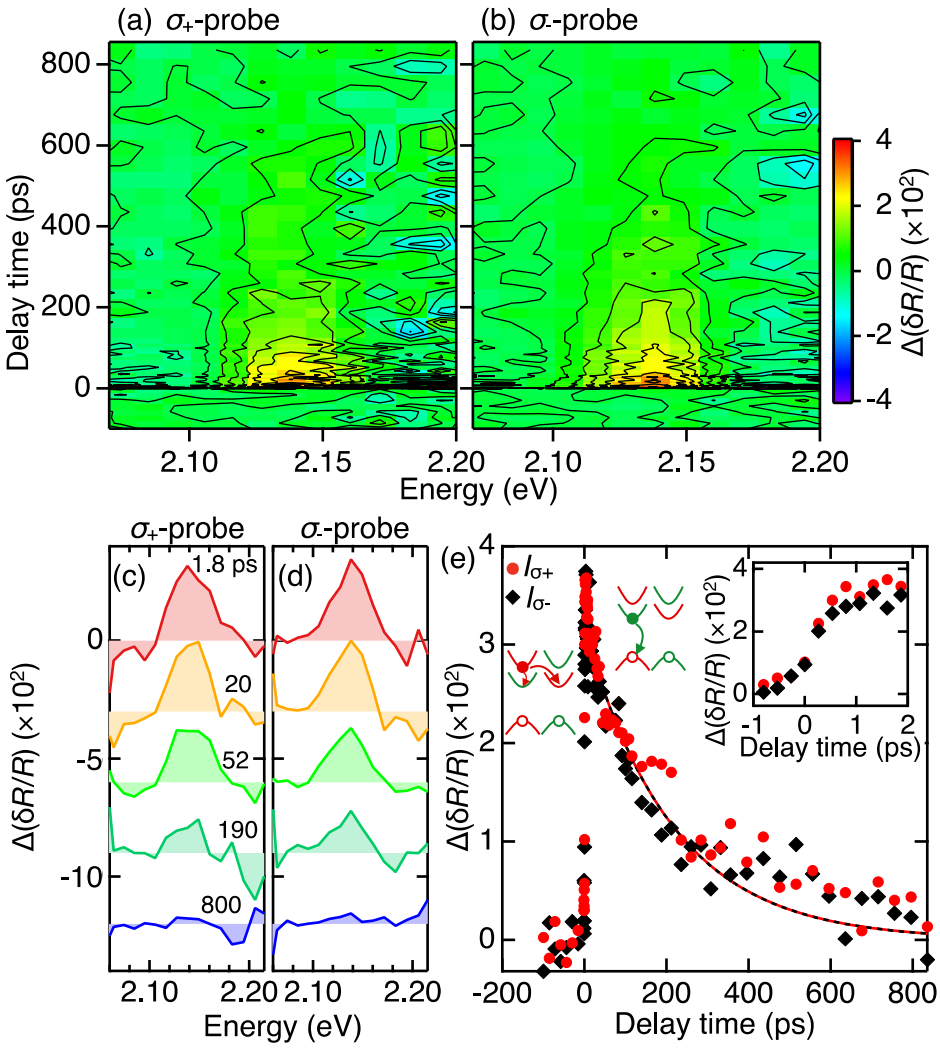

Figure 2 K. Shinokita *et al.*

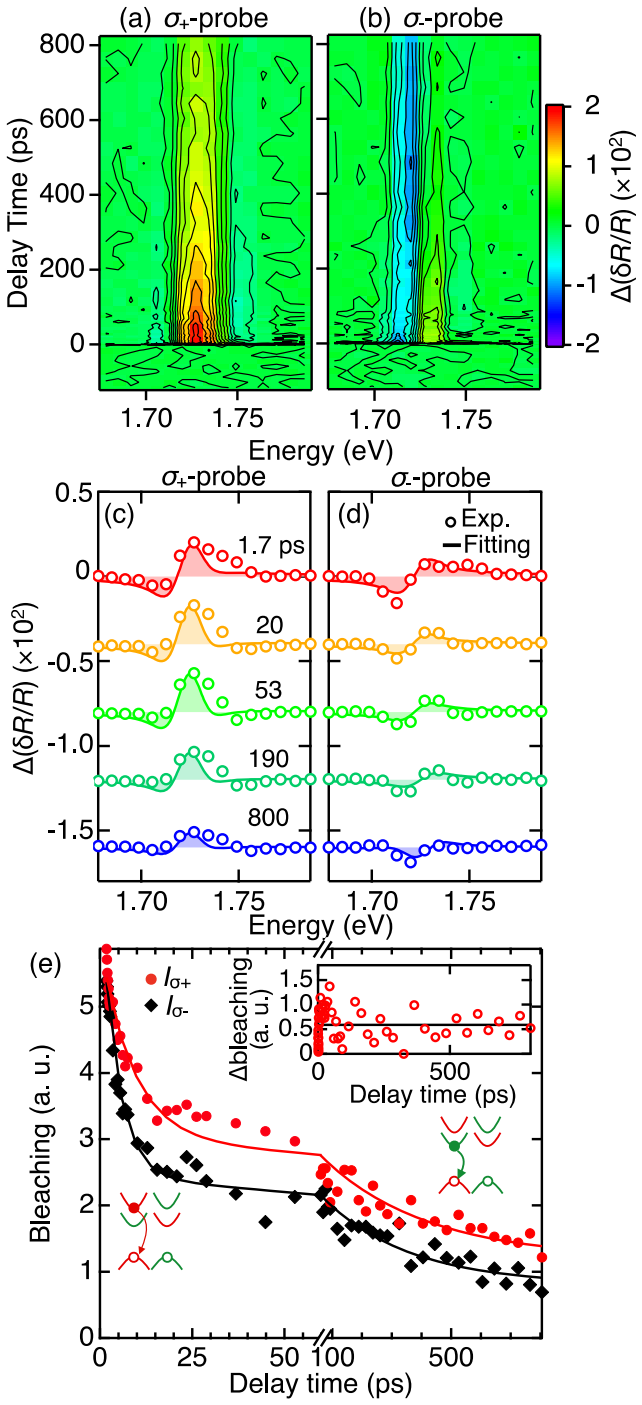

Figure 3 K. Shinokita *et al.*

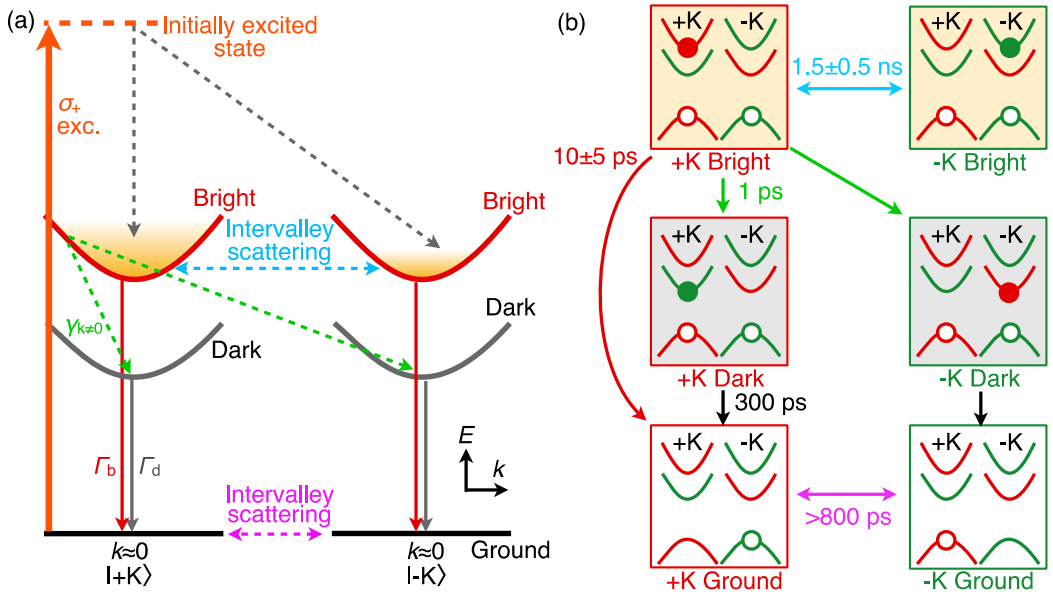

Figure 4 K. Shinokita *et al.*

References

[1] K.F. Mak, C. Lee, J. Hone, J. Shan, and T.F. Heinz, Phys. Rev. Lett. **105**, 136805 (2010).

[2] A. Splendiani, L. Sun, Y. Zhang, T. Li, J. Kim, C.Y. Chim, G. Galli, and F. Wang, Nano Lett. **10**, 1271 (2010).

[3] J.S. Ross, S. Wu, H. Yu, N.J. Ghimire, A.M. Jones, G. Aivazian, J. Yan, D.G. Mandrus, D. Xiao, W. Yao, and X. Xu, Nat. Commun. **4**, 1473 (2013).

[4] K.F. Mak, K. He, C. Lee, G.H. Lee, J. Hone, T.F. Heinz, and J. Shan, Nat. Mater. **12**, 207 (2013).

[5] A. Chernikov, T.C. Berkelbach, H.M. Hill, A. Rigosi, Y. Li, O.B. Aslan, D.R. Reichman, M.S. Hybertsen, and T.F. Heinz, Phys. Rev. Lett. **113**, 076802 (2014).

[6] K. He, N. Kumar, L. Zhao, Z. Wang, K.F. Mak, H. Zhao, and J. Shan, Phys. Rev. Lett. **113**, 026803 (2014).

[7] B. Zhu, X. Chen, and X. Cui, Sci. Rep. **5**, 9218 (2015).

[8] Y. Lin, X. Ling, L. Yu, S. Huang, A.L. Hsu, Y.H. Lee, J. Kong, M.S. Dresselhaus, and T. Palacios, Nano Lett. **14**, 5569 (2014).

[9] J. Yang, T. Lü, Y.W. Myint, J. Pei, D. Macdonald, J.C. Zheng, and Y. Lu, ACS Nano **9**, 6603 (2015).

[10] A. Boulesbaa, B. Huang, K. Wang, M.W. Lin, M. Mahjouri-Samani, C. Rouleau, K. Xiao, M. Yoon, B. Sumpter, A. Puretzky, and D. Geohegan, Phys. Rev. B **92**, 115443 (2015).

[11] S. Sim, J. Park, J.G. Song, C. In, Y.S. Lee, H. Kim, and H. Choi, Phys. Rev. B **88**, 075434 (2013).

[12] Y. Hoshi, T. Kuroda, M. Okada, R. Moriya, S. Masubuchi, K. Watanabe, T. Taniguchi, R. Kitaura, and T. Machida, Phys. Rev. B **95**, 241403(R) (2017).

[13] D. Xiao, G.-B. Liu, W. Feng, X. Xu, and W. Yao, Phys. Rev. Lett. **108**, 196802 (2012).

[14] K.F. Mak, K. He, J. Shan, and T.F. Heinz, Nat. Nanotechnol. **7**, 494 (2012).

[15] G. Wang, L. Bouet, D. Lagarde, M. Vidal, A. Balocchi, T. Amand, X. Marie, and B. Urbaszek, Phys. Rev. B **90**, 075413 (2014).

[16] A.T. Hanbicki, G. Kioseoglou, M. Currie, C.S. Hellberg, K.M. McCreary, A.L. Friedman, and B.T. Jonker, Sci. Rep. **6**, 18885 (2016).

[17] H. Zeng, J. Dai, W. Yao, D. Xiao, and X. Cui, Nat. Nanotechnol. **7**, 490 (2012).

[18] X. Xu, W. Yao, D. Xiao, and T.F. Heinz, Nat. Phys. **10**, 343 (2014).

[19] K.F. Mak, K.L. McGill, J. Park, and P.L. McEuen, Science **344**, 1489 (2014).

[20] R. Suzuki, M. Sakano, Y.J. Zhang, R. Akashi, D. Morikawa, A. Harasawa, K. Yaji, K.

Kuroda, K. Miyamoto, T. Okuda, K. Ishizaka, R. Arita, and Y. Iwasa, Nat. Nanotechnol. **9**, 611 (2014).
[21] T. Deilmann and K.S. Thygesen, Phys. Rev. B **96**, 201113(R) (2017).
[22] E. Courtade, M. Semina, M. Manca, M.M. Glazov, C. Robert, F. Cadiz, G. Wang, T. Taniguchi, K. Watanabe, M. Pierre, W. Escoffier, E.L. Ivchenko, P. Renucci, X. Marie, T. Amand, and B. Urbaszek, Phys. Rev. B **96**, 085302 (2017).
[23] H. Yu, X. Cui, X. Xu, and W. Yao, Natl. Sci. Rev. **2**, 57 (2015).
[24] M.R. Molas, C. Faugeras, A.O. Slobodeniuk, K. Nogajewski, M. Bartos, D.M. Basko, and M. Potemski, 2D Mater. **4**, 021003 (2017).
[25] X.X. Zhang, T. Cao, Z. Lu, Y.C. Lin, F. Zhang, Y. Wang, Z. Li, J.C. Hone, J.A. Robinson, D. Smirnov, S.G. Louie, and T.F. Heinz, Nat. Nanotechnol. **12**, 883 (2017).
[26] Y. Zhou, G. Scuri, D.S. Wild, A.A. High, A. Dibos, L.A. Jauregui, C. Shu, K. De Greve, K. Pistunova, A.Y. Joe, T. Taniguchi, K. Watanabe, P. Kim, M.D. Lukin, and H. Park, Nat. Nanotechnol. **12**, 856 (2017).
[27] K. Park, T. Jiang, G. Clark, X. Xu, and M.B. Raschke, Nat. Nanotechnol. **13**, 59 (2018).
[28] W. Zhao, Z. Ghorannevis, L. Chu, M. Toh, C. Kloc, P.-H. Tan, and G. Eda, ACS Nano **7**, 791 (2013).
[29] W. Zhao, Z. Ghorannevis, K.K. Amara, J.R. Pang, M. Toh, X. Zhang, C. Kloc, P.H. Tan, and G. Eda, Nanoscale **5**, 9677 (2013).
[30] J. Pu, T. Fujimoto, Y. Ohasi, S. Kimura, C.H. Chen, L.J. Li, T. Sakanoue, and T. Takenobu, Adv. Mater. **29**, 1606918 (2017).
[31] H. Zhong, Z. Zhang, H. Xu, C. Qiu, and L.M. Peng, AIP Adv. **5**, 057136 (2015).
[32] P.D. Cunningham, K.M. McCreary, and B.T. Jonker, J. Phys. Chem. Lett. **7**, 5242 (2016).
[33] A. Kormányos, G. Burkard, M. Gmitra, J. Fabian, V. Zólyomi, N.D. Drummond, and V. Fal'ko, 2D Mater. **2**, 022001 (2015).
[34] Z. Wang, A. Molina-Sánchez, P. Altmann, D. Sangalli, D. De Fazio, G. Soavi, U. Sassi, F. Bottegoni, F. Ciccacci, M. Finazzi, L. Wirtz, A.C. Ferrari, A. Marini, G. Cerullo, and S. Dal Conte, Nano Lett. **18**, 6882 (2018).
[35] G. Plechinger, P. Nagler, A. Arora, R. Schmidt, A. Chernikov, A.G. Del Águila, P.C.M. Christianen, R. Bratschitsch, C. Schüller, and T. Korn, Nat. Commun. **7**, 12715 (2016).
[36] A.M. Jones, H. Yu, N.J. Ghimire, S. Wu, G. Aivazian, J.S. Ross, B. Zhao, J. Yan, D.G. Mandrus, D. Xiao, W. Yao, and X. Xu, Nat. Nanotechnol. **8**, 634 (2013).
[37] Y. You, X.X. Zhang, T.C. Berkelbach, M.S. Hybertsen, D.R. Reichman, and T.F. Heinz, Nat. Phys. **11**, 477 (2015).

[38] W.T. Hsu, Y.L. Chen, C.H. Chen, P.S. Liu, T.H. Hou, L.J. Li, and W.H. Chang, Nat. Commun. **6**, 8963 (2015).
[39] C.H. Lui, A.J. Frenzel, D. V. Pilon, Y.H. Lee, X. Ling, G.M. Akselrod, J. Kong, and N. Gedik, Phys. Rev. Lett. **113**, 166801 (2014).
[40] See Supplemental Material at [URL will be inserted by publisher] for the energy shift of transient differential reflectance around A transition.
[41] P. Steinleitner, P. Merkl, P. Nagler, J. Mornhinweg, C. Schüller, T. Korn, A. Chernikov, and R. Huber, Nano Lett. **17**, 1455 (2017).
[42] Z. Nie, R. Long, L. Sun, C. Huang, J. Zhang, and Q. Xiong, ACS Nano **8**, 10931 (2014).
[43] D. Lagarde, L. Bouet, X. Marie, C.R. Zhu, B.L. Liu, T. Amand, P.H. Tan, and B. Urbaszek, Phys. Rev. Lett. **112**, 047401 (2014).
[44] G. Kioseoglou, A.T. Hanbicki, M. Currie, A.L. Friedman, D. Gunlycke, and B.T. Jonker, Appl. Phys. Lett. **101**, 221907 (2012).
[45] S. Konabe, Appl. Phys. Lett. **109**, 073104 (2016).
[46] Y. Miyauchi, S. Konabe, F. Wang, W. Zhang, A. Hwang, Y. Hasegawa, L. Zhou, S. Mouri, M. Toh, G. Eda, and K. Matsuda, Nat. Commun. **9**, 2598 (2018).
[47] See Supplemental Material at [URL will be inserted by publisher] for the estimation of initial valley polarization created by circularly polarized light.
[48] See Supplemental Material at [URL will be inserted by publisher] for the valley relaxation time at 50 K.
[49] E.A.A. Pogna, M. Marsili, D. De Fazio, S. Dal Conte, C. Manzoni, D. Sangalli, D. Yoon, A. Lombardo, A.C. Ferrari, A. Marini, G. Cerullo, and D. Prezzi, ACS Nano **10**, 1182 (2016).
[50] A. Chernikov, C. Ruppert, H.M. Hill, A.F. Rigosi, and T.F. Heinz, Nat. Photonics **9**, 466 (2015).
[51] Q.C. Sun, L. Yadgarov, R. Rosentsveig, G. Seifert, R. Tenne, and J.L. Musfeldt, ACS Nano **7**, 3506 (2013).
[52] See Supplemental Material at [URL will be inserted by publisher] for the effect of spin-polarized holes in energy shift.
[53] X. Song, S. Xie, K. Kang, J. Park, and V. Sih, Nano Lett. **16**, 5010 (2016).
[54] T. Yan, S. Yang, D. Li, and X. Cui, Phys. Rev. B **95**, 241406(R) (2017).
[55] P. Dey, L. Yang, C. Robert, G. Wang, B. Urbaszek, X. Marie, and S.A. Crooker, Phys. Rev. Lett. **119**, 137401 (2017).
[56] See Supplemental Material at [URL will be inserted by publisher] for the summary of the obtained timescales of bright and dark positive trions.

[57] C.R. Zhu, K. Zhang, M. Glazov, B. Urbaszek, T. Amand, Z.W. Ji, B.L. Liu, and X. Marie, Phys. Rev. B **90**, 161302(R) (2014).
[58] S. Dal Conte, F. Bottegoni, E.A.A. Pogna, D. De Fazio, S. Ambrogio, I. Bargigia, C. D'Andrea, A. Lombardo, M. Bruna, F. Ciccacci, A.C. Ferrari, G. Cerullo, and M. Finazzi, Phys. Rev. B **92**, 235425 (2015).
[59] C. Mai, A. Barrette, Y. Yu, Y.G. Semenov, K.W. Kim, L. Cao, and K. Gundogdu, Nano Lett. **14**, 202 (2013).
[60] M.M. Glazov, T. Amand, X. Marie, D. Lagarde, L. Bouet, and B. Urbaszek, Phys. Rev. B **89**, 201302(R) (2014).
[61] T. Yu and M.W. Wu, Phys. Rev. B **89**, 205303 (2014).
[62] C. Zhang, H. Wang, W. Chan, C. Manolatou, and F. Rana, Phys. Rev. B **89**, 205436 (2014).
[63] H. Yu, G. Bin Liu, P. Gong, X. Xu, and W. Yao, Nat. Commun. **5**, 3876 (2014).